Enahanced performance of BO_3^{3-}-doped $Li_3V_2(PO_4)_3$/C cathode materials synthesized via a controllable sol-gel method

Yu Zhang

College of Pharmacy, Xinjiang Medical University, Urumqi, 830011 Xinjiang, China
E-mail: 270478879@qq.com

BO_3^{3-}-doped $Li_3V_2(PO_4)_3$/C cathode materials with novel high-capacity performance are prepared by a controllable sol-gel method. X-ray diffraction and transmission electron microscopy are used to determine the microstructures and microscopic features of the materials. The electrochemical properties of the samples are characterized using constant current tests. The results demonstrate that the electrochemical performances of the materials can be greatly improved by the introduction of an appropriate quantity of boric acid. More specifically, with a doping content of 0.05, the discharge capacity of the material reaches 172.6 mAh·g^{-1} in the first week, with a rate of 0.2 C and a potential range 2–4.3 V. In addition, with an increase in the rate to 5 C, this material continue to maintain a high capacity of 121.4 mAh·g^{-1}. After 150 weeks of cycling at different rates, this material exhibits an initial capacity retention of 96.3%, thereby indicating its excellent capacity performance and stability.

1. INTRODUCTION

Due to ongoing economic globalization and the rising demand for energy, the search for new types of energy storage devices has become a hot topic [1–3]. In this context, lithium-ion batteries have been rapidly developed into new-generation energy storage devices due to their high specific energies, long cycle lives, small size, light weight, no memory effect, and environmental friendliness [4–6]. With the rapid development of portable electronic devices, the market scale of lithium-ion batteries is also expanding. Indeed, the application of lithium-ion batteries has not only allowed the evolution of small and lightweight electrical appliances, but it has also led to developments in large-scale electric equipment [7,8]. This has resulted in more demanding requirements for the capacity and stability of the cathode material. Therefore, the development of cathode materials with high charge-discharge capacities and good rate performances is essential for application in lithium-ion batteries. In recent years, lithium

vanadium phosphate cathode materials have been favored by researchers in the field of new energy materials because of their high capacities and good stabilities [9–11]. However, due to the structural characteristics of this material, defects exist, such as low electronic conductivity and poor rate performance, thereby limiting its further development and application [12–15]. It is therefore necessary to overcome these shortcomings relatively urgently. In previous studies, the doping of metal cations has been carried out [16–20], where these cations reduce the lattice order of the material by occupying the position of V^{3+} ions, thereby enhancing the conductivity and rate performance [21–24]. However, the majority of these metal ions do not exhibit electrochemical activity, which to some extent reduces the active substance content in the electrode, and weakens the capacity of the material [25, 26]. In contrast, anion doping can avoid this problem and improve the electrochemical performance of the material as a whole.

Thus, we herein report our investigation into the effect of boric acid doping (1–7%) on $Li_3V_2(PO_4)_3$/C materials by examination of the resulting morphologies and electrochemical properties of the doped materials. Ultimately, through optimization of the doping ratio, we aim to enhance the discharge capacities, conductivities, and rate performances of the prepared materials.

2. EXPERIMENTAL DETAILS

The doped samples were prepared by a simple and controllable sol-gel method. More specifically, the raw materials, namely $CH_3COOLi \cdot 2H_2O$, V_2O_5, H_3PO_4, H_3BO_3, and citric acid, were mixed in molar ratio of 3.15:1:(3−x):x:(1−0.5x), where the values of x were 0, 0.01, 0.03, 0.05, and 0.07. The chemical reagents used in the experiment are all analytical pure, from Tianjin Zhiyuan Chemical Reagents Co., Ltd. Details regarding the preparation of this mixture are as follows. Initially, the desired quantity of V_2O_5 was dissolved in deionized water (20 mL), and then H_2O_2 was added slowly dropwise with continuous stirring until an orange-red transparent solution was obtained. Subsequently, $CH_3COOLi \cdot 2H_2O$ was added to the above solution, and the resulting mixture stirred for 30 min to give a yellow transparent solution. Finally, citric acid, H_3PO_4, and H_3BO_3 were dissolved in deionized water (60 mL), and the resulting solution was stirred thoroughly prior to adding slowly dropwise to the above-mentioned yellow solution. This resulted in the formation of a deep red-colored solution after continuous stirring for 2 h. The obtained solution was then placed in a drying box and dried at 90 °C for 12 h to give a green solid, which was ground into a powder, pre-sintered at 350 °C for 4 h, then sintered at 800 °C for 12 h in a tube furnace under a flowing Ar atmosphere. The desired $Li_3V_2(PO_4)_{3-x}(BO_3)_x$/C (x = 0, 0.01, 0.03, 0.05, or 0.07) samples were obtained after cooling the above powder to room temperature and grinding.

The as-prepared samples were then subjected to X-ray diffraction measurements (XRD, Bruker D2) using Cu-Kα radiation. The morphology of the material was characterized by transmission electron microscopy (TEM, Philips CM10), and the electronic states of the elements were assessed by X-ray photoelectron spectroscopy (XPS, ESCALAB 250Xi).

The electrodes were obtained by mixing the active material, acetylene black, and polytetrafluoroethylene (PTFE) in a weight ratio of 80:15:5. The mixed slurry was then evenly coated

on aluminum foil, dried at room temperature, cut into slices with diameters of 10 mm, and dried under vacuum at 110 °C for 12 h. Lithium slices were used as the anode, the prepared $Li_3V_2(PO_4)_{3-x}(BO_3)_x/C$ materials were employed as the cathodes, a PP/PE/PP composite diaphragm was used as a separator, and a 1 M solution of $LiPF_6$ in a mixture of ethylene carbonate and dimethyl carbonate (1:1 by volume) was employed as the electrolyte. Finally, the two-electrode electrochemical cells were assembled in an argon-filled glove box. The cycle lives of the cells were evaluated using a battery test instrument (LAND, CT-2001A) at different rates (i.e., 0.2, 0.5, 1, 2, and 5 C) in the voltage range 2–4.3 V. Cyclic voltammetry (CV) and electrochemical impedance spectroscopy (EIS) measurements were carried out by means of an electrochemical workstation (LK2005A) following the electrochemical tests.

3. RESULTS AND DISCUSSION

Following preparation of the various materials containing different doping ratios, their microstructures were investigated by XRD (Fig. 1(a)). As can be seen in the figure, the patterns obtained for all modified samples were similar to that of the bare $Li_3V_2(PO_4)_3/C$ material, indexing the monoclinic crystal structure; this result is consistent with previous literature reports [27, 28].
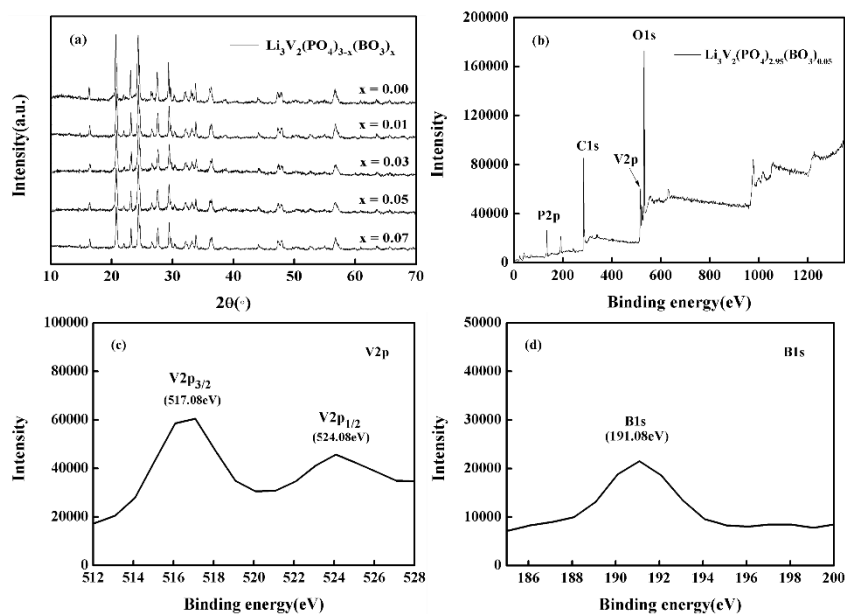

Figure 1. (a) X-ray diffraction patterns of the samples; (b) XPS survey spectra of the $Li_3V_2(PO_4)_{2.95}(BO_3)_{0.05}/C$ composite; (c) and (d) enlarged diagrams over the ranges of 512–528 eV and 185–205 eV, respectively.

More specifically, the XRD patterns of all samples contained identical peaks of high intensities, and no other diffraction peaks corresponding to impurities or carbon were observed, thereby confirming the pure phase of each prepared material in addition to indicating the amorphous nature of the carbon coating. To further explore the internal elemental composition of the material, XPS was carried out.

Taking the XPS survey spectrum of the $Li_3V_2(PO_4)_{3-x}(BO_3)_x/C$ (x = 0.05) composite as an example (Fig. 1(b)), the binding energies on the different orbits of P, C, V, and O could be roughly obtained. Thus, Figs. 1(c) and 1(d) show magnified images in the binding energy ranges 512–528 eV and 185–200 eV, respectively. As indicated, two obvious peaks were observed at binding energies of 517.08 and 524.08 eV, which correspond to the $2p_{3/2}$ and V $2p_{1/2}$ orbits respectively, indicating that the valence of V in the material is +3 [29, 30]. Similarly, the peak at a binding energy of 191.08 eV corresponded to the B1s orbital energy, which is consistent with the measurement tested in B_2O_3 [31], thereby indicating that the valence of B in H_3BO_3 (i.e., +3) did not change during the synthetic process. These results therefore confirmed the successful preparation of pure phase $Li_3V_2(PO_4)_{3-x}(BO_3)_x/C$ materials. The morphologies of the materials were examined by TEM, where Figs. 2(a) and 2(b) show the TEM images of the bare and $Li_3V_2(PO_4)_{3-x}(BO_3)_x/C$ (x = 0.05) materials, respectively, with a unit size of 50 nm. In addition, Figs. 2(c) and 2(d) show high-resolution transmission electron microscopy (HRTEM) images of the two materials, with a unit size of 5 nm. These images confirm that the synthesized materials are regular spherical particles ranging in size from 50–200 nm and 20–100 nm, respectively, thereby indicating that the morphology and size of the material can be controlled by the synthetic method employed herein. Furthermore, the spherical nature of this material is of particular importance for its application, since it results in increased specific surface areas, increased contact areas between the material and the electrolyte, and a reduction in the degree of aggregation of the material. It is also apparent that the particle size of the doped material is significantly smaller than that of the pure $Li_3V_2(PO_4)_3/C$ material, which effectively shortens the Li^+ migration path during the redox process.
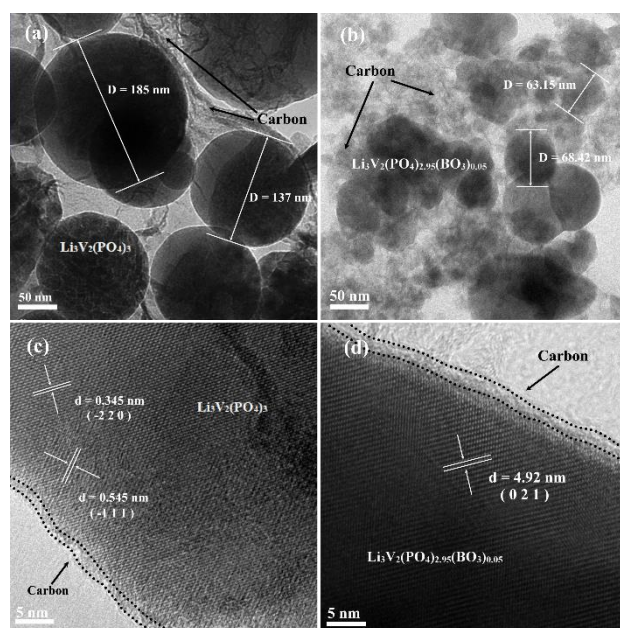

Figure 2. TEM images of the bare and $Li_3V_2(PO_4)_{3-x}(BO_3)_x/C$(x = 0.05) materials(a and b: unit size of 50nm; c and d: unit size of 5nm).

This morphology therefore plays an important role in improving the capacity properties of the prepared materials. Moreover, upon examination of Figs. 2(c) and 2(d), a uniform amorphous carbon

film can be observed on the surfaces of the bare and doped material, respectively, which is consistent with the results obtained by XRD. We also note that three different lattice fringes were captured in two images, and comparison with the standard PDF card of $Li_3V_2(PO_4)_3$ allowed determination of the crystal faces of the fringes, as annotated in the figure. Again, these results further confirm the pure phases of the synthesized materials.

Figure 3 shows the first cycle charge-discharge curves of the different materials at a rate of 0.2 C and a voltage range 2–4.3 V. More specifically, curves a, b, c, d, and e represent the materials with doping ratios of x = 0, 0.01, 0.03, 0.05, and 0.07, respectively. From this figure, we can see that the pure $Li_3V_2(PO_4)_3$/C material has three pairs of obvious charging and discharging platforms; these represent the redox processes of the first two lithium ions in the material under low voltage conditions [32, 33]. However, upon the introduction of BO_3^{3-} ions into the material, the platforms changed from three pairs to essentially two pairs due to the fact that the total charge of BO_3^{3-} is less than that of PO_4^{3-}, and so the first charging platforms of the materials are reduced. Furthermore, to compensate for the loss of charge balance, the materials are converted into more high valence substances during the oxidation processes, and the second charging platforms of the materials are significantly increased. This effect mainly occurs in the insertion/deinsertion processes of the first lithium ion in the material. Based on our results, the special discharge capacities of the materials where x = 0, 0.01, 0.03, 0.05, and 0.07 were determined to be 127.9, 158.2, 164.9, 172.6, and 140.7 mAh·g^{-1}, respectively. It was therefore apparent that the capacity of bare material was similar to the theoretical capacity, which may be attributed to the special morphology of the material. Moreover, it can be seen that the capacity properties of the doped materials were greatly improved, likely due to a greater number of high valence substances being produced during the charging process, and the transformation of a greater number of low valence substances during the discharge process, thereby releasing a greater capacity. These assumptions are consistent with the information transmitted by the discharge platform of the material.
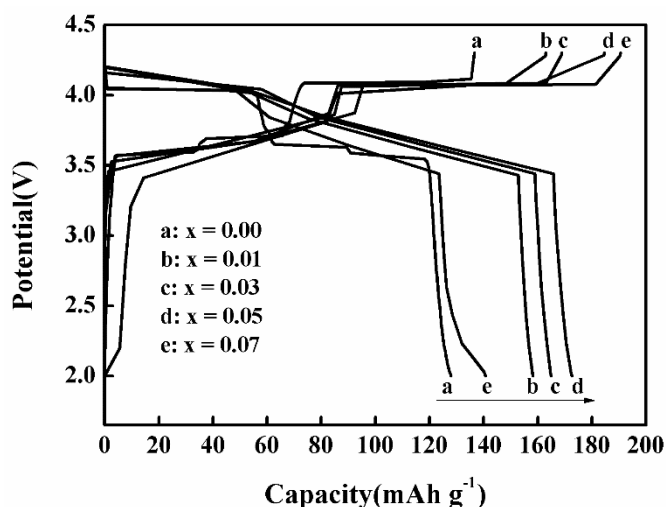

Figure 3. The first charge-discharge curves of the synthesized composites at the rate of 0.2 C and in the potential range of 2.0 - 4.3 V.

To further investigate the rate performances of the prepared materials, they were tested over 150

cycles under rates of 0.2, 0.5, 1, 2, and 5 C (Fig. 4). As indicated, the discharge capacities of all doped materials increased under high rate conditions, thereby confirming an enhancement in their rate performances. For a clear comparison of the rate performances of the various materials, the obtained experimental data are presented in Table 1. More specifically, at rates of 0.2 and 5C, the first cycle discharge capacities of the bare material are 127.9 and 61.5 mAh·g^{-1}, respectively, indicating that the pure $Li_3V_2(PO_4)_3$/C material has a high first cycle discharge capacity, but that this decreases rapidly upon increasing the rate, reflecting a poor rate performance. In contrast, at rates of 0.2 and 5 C, the discharge capacities of the doped materials (where x = 0.01, 0.03, 0.05, and 0.07) are 158.2, 164.9, 172.6, and 140.7 mAh·g^{-1} and 98.0, 104.9, 121.4, and 93.5 mAh·g^{-1}, respectively. These results indicate that to a certain extent, the addition of boric acid can improve the rate performance of the material, with an optimal doping ratio of 0.05 being determined, where the $Li_3V_2(PO_4)_{2.95}(BO_3)_{0.05}$/C material exhibits the best high-rate discharge capacity.
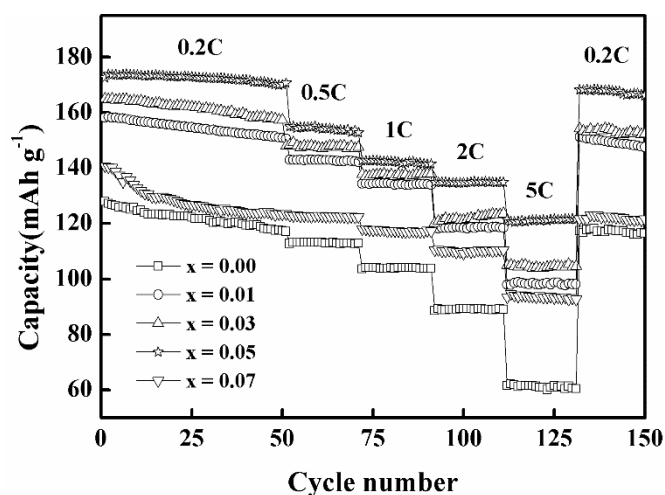

Figure 4. The special discharge capacities of the materials at different rates(0.2, 0.5, 1, 2 and 5 C) between 2 and 4.3 V.
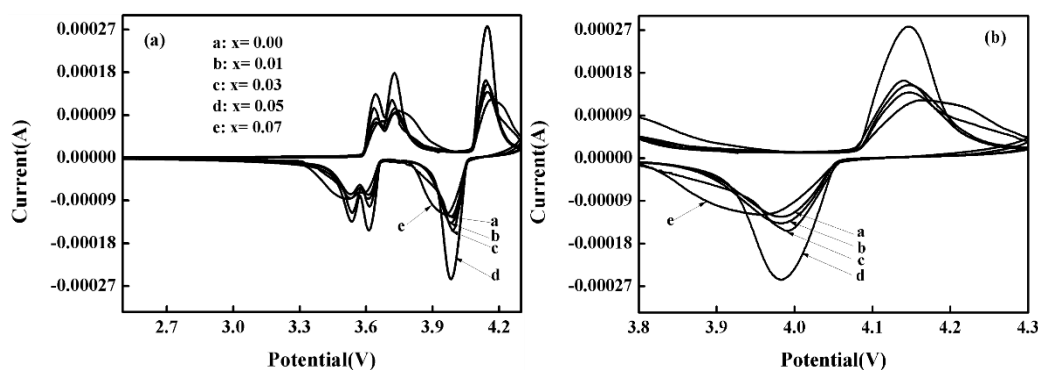
Table 1. Comparison of discharge capacities of synthesized materials at different rates in the voltage range of 2–4.3V.

Sample	Discharge capacity (mAh·g^{-1})				
	0.2C	0.5C	1C	2C	5C
$Li_3V_2(PO_4)_3$/C	127.9	112.8	103.6	88.5	61.5
$Li_3V_2(PO_4)_{2.99}(BO_3)_{0.01}$/C	158.2	143.1	134.4	118.5	98.0
$Li_3V_2(PO_4)_{2.97}(BO_3)_{0.03}$/C	164.9	148.4	137.8	120.2	104.9
$Li_3V_2(PO_4)_{2.95}(BO_3)_{0.05}$/C	172.6	155.0	142.7	134.9	121.4
$Li_3V_2(PO_4)_{2.93}(BO_3)_{0.07}$/C	140.7	123.0	118.0	110.4	93.5

Table 2. comparison of the performance of various modified $Li_3V_2(PO_4)_3/C$ cathode materials.

Sample	Rate (C)	Voltage range (V)	Discharge capacity (mAh·g^{-1})	Reference
K-doped $Li_3V_2(PO_4)_3/C$	0.1	3.0–4.3	140.0	[16]
Ge-doped $Li_3V_2(PO_4)_3/C$	0.2	2.0–4.3	137.2	[18]
Fe-doped $Li_3V_2(PO_4)_3/C$	1.0	3.0–4.8	142.5	[19]
Nd^{3+}-doped $Li_3V_2(PO_4)_3/C$	0.2	3.0–4.3	115.1	[20]
Mg-doped $Li_3V_2(PO_4)_3/C$	0.1	3.0–4.3	146.0	[22]
Pd^{2+} and BO_3^{3-} co-doped $Li_3V_2(PO_4)_3/C$	0.2	2.0-4.3	159.2	[23]
BO_3^{3-}-doped $Li_3V_2(PO_4)_3/C$	0.2	2.0–4.3	172.6	This work

A comparison of rates, voltage ranges, and discharge capacities for various modified $Li_3V_2(PO_4)_3/C$ cathode materials reported in literature was shown in table 2. In general, under the condition of low rate and high charging voltage, the material can deliver good electrochemical performance, especially the high discharge capacity. It can be seen from the comparison that even have a favorable condition for electrochemical properties, the cation doped $Li_3V_2(PO_4)_3/C$ materials still release lower discharge capacity. In this study, single anion doping is used. Under the same conditions, it has made remarkable progress. When at lower charging voltage and higher rate, the material emerges excellent discharge capacity, which is due to the fact that single anion doping can increase the conductivity, reduce the particle size and effectively improve the electrochemical performance of the material without affecting the active material content. This discovery can provide theoretical basis for the application of large power supply in the future.

Figure 5. (a) CV curves of as-prepared composites in the potential range of 2–4.3V with a scan rate of 0.1mV s^{-1} after 150 cycles; (b) is an enlarged view of a voltage range of 3.8–4.3V.

Another means to explore the internal redox mechanism and the stability of a material is CV, and so the CV curves of the various materials were obtained after 150 cycles at different rates under a voltage range 2–4.3 V and a scan rate of 0.1 mV·s^{-1} (Fig. 5(a)). As shown, all materials exhibit three pairs of redox peaks, corresponding to the three redox processes taking place within the materials, and this result

is consistent with the number of charging/discharging platforms previously described for the various samples. Taking the redox peak in the voltage range 3.8–4.3 V as an example, the redox peak strength and the peak current values of the different materials were carefully compared. As shown in Fig. 5(b), where curves a, b, c, d, and e represent materials with doping ratios x = 0, 0.01, 0.03, 0.05, and 0.07, respectively, with a doping ratio of <0.07, the redox voltage difference decreases and the peak current value increases, indicating that an appropriate level of doping can enhance the stability of the material. More specifically, at a doping ratio of 0.05, the largest redox peak current is obtained, indicating that this material exhibits the best reversibility. However, upon increasing the doping ratio to 0.07, the peak voltage difference increases and the peak current decreases, thereby indicating that an excess of BO_3^{3-} ions will reduce the stability of the material. This can be attributed to the fact that the excess introduction of foreign ions with smaller ionic radii can cause damage to the structure of the material, which is not conducive to its stability.
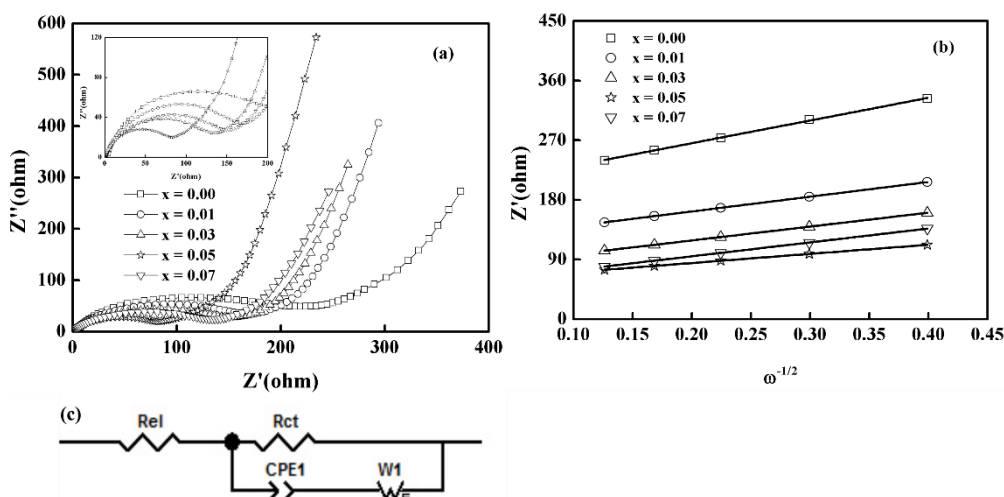

Figure 6. (a) Nyquist plots for the EIS of the electrodes;(b) relationship between Z_{re} and $\omega^{-1/2}$ at low frequencies; (c) equivalent circuit of the experimental data.

Table 3. $Li_3V_2(PO_4)_{3-x}(BO_3)_x$/C cathode electrodes kinetic parameters obtained from equivalent circuit fitting of experimental data.

Sample	$R_e(\Omega)$	$R_{ct}(\Omega)$	$D(cm^2 \cdot s^{-1})$
$Li_3V_2(PO_4)_3$/C	3.24	220.80	3.30×10^{-12}
$Li_3V_2(PO_4)_{2.99}(BO_3)_{0.01}$/C	2.21	193.85	6.26×10^{-12}
$Li_3V_2(PO_4)_{2.97}(BO_3)_{0.03}$/C	2.01	183.33	8.12×10^{-12}
$Li_3V_2(PO_4)_{2.95}(BO_3)_{0.05}$/C	1.38	87.40	9.34×10^{-12}
$Li_3V_2(PO_4)_{2.93}(BO_3)_{0.07}$/C	1.81	160.02	8.73×10^{-12}

R_e: uncompensated resistance; R_{ct}: charge transfer resistance; D: lithium diffusion coefficient

To further explore the electrochemical behavior of each prepared material, the electrochemical kinetic parameters were examined by EIS after 150 cycles in the potential range 2–4.3 V. As shown in Fig. 6(a), the compositions of the resulting Nyquist plots were comparable for all materials. In addition, Fig. 6(b) shows the relationship between impedance (Z_{re}) and the angular frequency ($\omega^{-1/2}$) in the low frequency region, while Fig. 6(c) shows the equivalent circuit used to fit the experimental data. Thus, the kinetic data of various materials were calculated and listed in Table 2 [34–36]. After careful comparison, it can be found that the charge transfer impedance of the undoped material is 220.80 Ω, while upon the introduction of BO_3^{3-} ions, the charge transfer impedance decreased significantly, giving values of 193.85, 183.33, 87.40, and 160.02 Ω for x = 0.01, 0.03, 0.05, and 0.07, respectively. This can be accounted for by considering that the introduction of foreign ions with a low ionic radius reduces the lattice order and enhances the conductivity of the material, which effectively improves the rate performance. It is also apparent that the lithium ion mobility of the doped materials was significantly improved following doping, which was attributed not only to the increase in the conductivity of each material, but also to the decrease in particle size. This in turn will effectively improve the discharge capacity, which is consistent with the above observations. Overall, our results indicate that $Li_3V_2(PO_4)_{2.95}(BO_3)_{0.05}/C$ exhibits the lowest uncompensated impedance and charge transfer impedance, and the largest ion mobility, thereby indicating that the optimal doping ratio of the BO_3^{3-} ion is x = 0.05.

4. CONCLUSIONS

We herein reported the preparation of $Li_3V_2(PO_4)_{3-x}(BO_3)_x/C$ cathode materials with different doping ratios (x = 0, 0.01, 0.03, 0.05, and 0.07) via a controllable sol-gel method using BO_3^{3-} ions as the doping species. Our results indicated that this method of modification can have a large effect on the properties of $Li_3V_2(PO_4)_3/C$ materials, and in particular, it can significantly enhance their electrochemical properties. In addition, observations by transmission electron microscopy showed that regular spherical materials can be synthesized by this method, and that the particle size of the materials could be significantly reduced by the introduction of BO_3^{3-} ions. The special morphology also increases the contact area between the material and the electrolyte, reduces the agglomeration degree of the material, shortens the lithium-ion migration path, enhances the diffusion of lithium ions, and significantly improves the discharge capacities of the materials. Furthermore, the results of electrochemical performance tests showed that the introduction of a low-radius and low-charge ion reduces the lattice order of the material, in addition to effectively enhancing the conductivity, and improving the rate performance. Overall, we found that the optimum doping ratio of BO_3^{3-} ions was x = 0.05, where at rates of 0.2 and 5 C, the special discharge capacity of this material (i.e., $Li_3V_2(PO_4)_{2.95}(BO_3)_{0.05}/C$) reached 172.6 and 121.4 mAh·g^{-1}, respectively, in the potential range 2–4.3 V. Moreover, after 150 weeks of cycling at different rates, the initial capacity retention rate of the material was 96.3%, thereby confirming its excellent capacity performance and stability, and highlighting the potential of this material for use as a superior cathode material in lithium-ion batteries.

References

1. G.E. Blomgren, *J. Electrochem. Soc.*, 164 (2017) A5019.
2. D.C. Lin, Z.D. Lu, P.C. Hsu, H.R. Lee, N. Liu, J. Zhao, H.T. Wang, C. Liu, Y. Cui, *Energy Environ. Sci.*, 8 (2015) 2371.
3. M. Ko, S. Chae, J.Y. Ma, N. Kim, H.R. Lee, Y. Cui, J. Cho, *Nat. Energy*, 1 (2016) 16113.
4. Z.Y. Tu, P. Nath, Y.Y. Lu, M.D. Tikekar, L.A. Archer, *Acc. Chem. Res.*, 48 (2015) 2947.
5. T.M. Higgins, S.H. Park, P.J. King, C.F. Zhang, N. MoEvoy, N.C. Berner, D. Daly, A. Shmeliov, U. Khan, G. Duesberg, V. Nicolosi, J.N. Coleman, *Acs Nano*, 10 (2016) 3702.
6. Y. Liu, W.L. Yao, C. Lei, Q. Zhang, S.W. Zhong, Z.Q. Yan, *J. Electrochem. Soc.*, 166 (2019) A1300.
7. M. Haruta, T. Doi, M. Inaba, *J. Electrochem. Soc.*, 166 (2019) A258.
8. V. Etacheri, R. Marom, R. Elazari, G. Salitra, D. Aurbach, *Energy Environ. Sci.*, 4 (2011) 3243.
9. H.T. Tan, L.H. Xu, H.B. Geng, X.H. Rui, C.C. Li, S.M. Huang, *Small*, 14 (2018) 1800567.
10. L.L. Zhang, Z. Li, X.L. Yang, X.K. Ding, Y.X. Zhou, H.B. Sun, H.C. Tao, L.Y. Xiong, Y.H. Huang, *Nano Energy*, 34 (2017) 111.
11. S.Q. Liang, X.X. Cao, Y.P. Wang, Y. Hu, A.Q. Pan, G.Z. Cao, *Nano Energy*, 22 (2016) 48.
12. K. Cui, S.C. Hu, Y.K. Li, *Electrochim. Acta*, 210 (2016) 45.
13. W.F. Mao, Y.B. Fu, H. Zhao, G. Ai, Y.L. Dai, D.C. Meng, X.H. Zhang, D.Y. Qu, G. Liu, V.S. Battaglia, *ACS Appl. Mater. Interfaces*, 7 (2015) 12057.
14. Q. Liu, L.B. Ren, C.J. Cong, F. Ding, F.X. Guo, D.W. Song, J. Guo, X.X. Shi, L.Q. Zhang, *Electrochim. Acta*, 187 (2016) 264.
15. Y.X. Liao, C. Li, X.B. Lou, X.S. Hu, Y.Q. Ning, F.Y. Yuan, B. Chen, M. Shen, B.W. Hu, *Electrochim. Acta*, 271 (2018) 608.
16. L. Jiang, C.P. Fu, K.Q. Li, H.H. Zhou, Y.P. Huang, Y.F. Kuang, *Mater. Lett.*, 198 (2017) 73.
17. M.M. Ren, M.Z. Yang, W.L. Liu, M. Li, L.W. Su, X.B. Wu, Y.H. Wang, *J. Power Sources*, 326 (2016) 313.
18. Y. Zhang, Z. Su, J. Ding, *J. Alloys Compd.*, 702 (2017) 427.
19. Z.Q. Cao, C.Y. Zuo, X.M. Cui, X.F. Zhang, *Ionics*, 25 (2019) 5709.
20. Y.J. Li, C.X. Zhou, S. Chen, F. Wu, L. Hong, *Chin. Chem. Lett.*, 26 (2015) 1004.
21. Y. Kee, N. Dimov, E. Kobayashi, A. Kitajou, S. Okada, *Solid State Ionics*, 272 (2015) 138.
22. Y.Z. Luo, L.H. He, X.H. Liu, *Trans. Nonferrous Met. Soc. China*, 25 (2015) 2266.
23. Y. Zhang, *RSC Adv.*, 9 (2019) 25942.
24. D. Okada, F. Nakano, K. Uematsu, H. Okawa, A. Itadani, K. Toda, M. Sato, *Electrochem.*, 83 (2015) 828.
25. W.M. Yin, T.T. Zhang, Q. Zhu, Q.Q. Chen, G.C. Li, L.Z. Zhang, *Trans. Nonferrous Met. Soc. China*, 25 (2015) 1978.
26. J.S. Park, J. Kim, W.B. Park, Y.K. Sun, S.T. Myung, *ACS Appl. Mater. Interfaces*, 9 (2017) 40307.
27. C. Wang, Z.Y. Guo, W. Shen, A.L. Zhang, Q.J. Q.J. Xu, Y.G. Wang, *J. Mater. Chem. A*, 3 (2015) 6064.
28. X.M. Cui, T.T. Liu, *Ionics*, 25 (2019) 3603.
29. J.C. Zheng, X.H. Li, Z.X. Wang, H.J. Guo, Q.Y. Hu, W.J. Peng, *J. Power Sources*, 189 (2009) 476.
30. M.M. Ren, Z. Zhou, Y.Z. Li, X.P. Gao, J. Yan, *J. Power Sources*, 162 (2006) 1357.
31. J.S. Huang, L. Yang, K.Y. Liu, *Mater. Chem. and Phys.*, 128 (2011) 470.
32. M.Y. Saıdi, J. Barker, H. Huang, *J. Power Sources*, 119 (2003) 266.
33. S.C. Yin , H. Grondey, P. Strobel, H. Huang, L.F. Nazar, *J. Am. Chem. Soc.*, 125 (2003) 326.

34. Y.C. Si, Z. Su, Y.B. Wang, T. Ma, *New J. Chem.*, 39 (2015) 8971.
35. Y.S. Hu, X. Ma, P. Guo, *J. Alloys Compd.*, 723 (2017) 873.
36. Z. Li, L.L. Zhang, X.L. Yang, H.B. Sun, Y.H. Huang, G. Liang, *RSC Adv.*, 6 (2016) 10334.